

A 90° mixed-mode twisted nematic liquid-crystal-on-silicon with an insulating protrusion structure

Wen-Juan Li(李文娟), Yu-Qiang Guo(郭玉强), Chi Zhang(张弛), Hong-Mei Ma(马红梅), and Yu-Bao Sun(孙玉宝)
Citation: Chin. Phys. B, 2021, 30 (**6**): 064210. DOI: 10.1088/1674-1056/abee0b
Journal homepage: http://cpb.iphy.ac.cn; http://iopscience.iop.org/cpb

What follows is a list of articles you may be interested in

Unidirectional plasmonic Bragg reflector based on longitudinally asymmetric nanostructures

Mingsong Chen(陈名松), Lulu Pan(潘璐璐), Yuanfu Lu(鲁远甫), Guangyuan Li(李光元)
Chin. Phys. B, 2019, 28 (**7**): 074208. DOI: 10.1088/1674-1056/28/7/074208

Active hyperspectral imaging with a supercontinuum laser source in the dark

Zhongyuan Guo(郭中源), Yu Liu(刘煜), Xin Zheng(郑鑫), Ke Yin(殷科)
Chin. Phys. B, 2019, 28 (**3**): 034206. DOI: 10.1088/1674-1056/28/3/034206

Analysis of optical properties of bio-smoke materials in the 0.25-14 μm band

Xinying Zhao(赵欣颖), Yihua Hu(胡以华), Youlin Gu(顾有林), Xi Chen(陈曦), Xinyu Wang(王新宇), Peng Wang(王鹏), Xiao Dong(董骁)
Chin. Phys. B, 2019, 28 (**3**): 034201. DOI: 10.1088/1674-1056/28/3/034201

Enhancement and control of the Goos-Hänchen shift bynonlinear surface plasmon resonance in graphene

Qi You(游琪), Leyong Jiang(蒋乐勇), Xiaoyu Dai(戴小玉), Yuanjiang Xiang(项元江)
Chin. Phys. B, 2018, 27 (**9**): 094211. DOI: 10.1088/1674-1056/27/9/094211

Structural, vibrational, optical, photoluminescence, thermal, dielectric, and mechanical studies on zinc (tris) thiourea sulfate single crystal: A noticeable effect of organic dye

Mohd Shkir, V Ganesh, S AlFaify, I S Yahia, Mohd Anis
Chin. Phys. B, 2018, 27 (**5**): 054216. DOI: 10.1088/1674-1056/27/5/054216

A 90° mixed-mode twisted nematic liquid-crystal-on-silicon with an insulating protrusion structure*

Wen-Juan Li(李文娟)[1,2], Yu-Qiang Guo(郭玉强)[3], Chi Zhang(张弛)[1], Hong-Mei Ma(马红梅)[2], and Yu-Bao Sun(孙玉宝)[1,2,†]

[1] School of Electronic and Information Engineering, Hebei University of Technology, Tianjin 300401, China
[2] Department of Applied Physics, Hebei University of Technology, Tianjin 300401, China
[3] School of Instrumentation Science and Opto-electronics Engineering, Beihang University, Beijing 100191, China

(Received 15 February 2021; revised manuscript received 9 March 2021; accepted manuscript online 12 March 2021)

A 90° mixed-mode twisted nematic liquid-crystal-on-silicon (90°-MTN LCoS) with protrusion located between the adjacent pixels is proposed to reduce the effect of fringing field. The influence of the protrusion with different widths from 0.5 μm to 0.9 μm and different heights from 0.3 μm to 0.7 μm is investigated. The results demonstrate that the invalid pixel region width can be reduced by 31.5% via using the protrusion with the suitable width and height compared with no protrusion case, which provides a higher display quality, such as the higher reflectance and contrast ratio.

Keywords: liquid-crystal-on-silicon, mixed-mode twisted nematic, fringing field effect, reflectance

PACS: 42.79.Kr, 42.70.Df, 42.25.Gy **DOI:** 10.1088/1674-1056/abee0b

1. Introduction

Nowadays, with the advent of 5G,[1] the intelligent wearable devices have been put forward, especially the next generation wearable devices: near-eye display in virtual reality (VR). Against this backdrop, it requires fast response speed and high resolution to realize super image quality.[2–4] Organic light emission display (OLED) was thought to be suitable for the screen of virtual reality head mount displays (VR-HMD) because of its fast response speed.[5] However, it is difficult to obtain high resolution. The deposition of the OLED RGB emission layer was done through a metal mask. Small pixel pitch is required to obtain high-definition images, so the reducing pixel size is conceptually a straightforward way to increase the resolution of display.[6–8] Liquid-crystal-on-silicon (LCoS)[9] has been used extensively in near-eye virtual reality displays in micro-displays.[6,10–18] High resolution LCoS can be fabricated based on the high electron mobility of crystalline silicon.[19] However, with the decreasing of pixel size in the high-resolution LCoS device, the fringe field-effect between adjacent pixels becomes obvious.[20–26] It is difficult to drive one individual pixel because of the electric field leakage and penetration of the LC elastic force into adjacent pixels.[27] The fringing field can influence the liquid crystal distribution in the adjacent pixels, and ultimately degrade the optical performance severely.[28,29] To overcome this problem, several approaches have been pointed out, such as Eq. (1) employing weak fringing field effect liquid crystal mode: mixed-mode twist nematic (MTN).[30–32] The light propagation in MTN-LCoS combines the polarization rotation and birefringence effects,[33,34] so it not only shows the advantage of weak fringing field effect, but also shows high reflectance and low operation voltage. Equation (2) optimizing the structure of LCoS cell: the low dielectric constant polymer wall has been proposed to isolate the pixels in the LC cell,[34] and the dielectric shield wall structure and lattice-shaped dielectric walls have been proposed[27,35] as well. These structures can significantly reduce the fringing field effect of the LCoS device.

In this paper, we will propose a protrusion located between the adjacent pixels in the high-resolution LCoS device, analyze the effect of the protrusion in the voltage-on pixel and the adjacent voltage-off pixels in 90°-MTN mode, and investigate the fringe field effect. The invalid pixel region is proposed to define the fringe field effect. The results show that the protrusion between the adjacent pixels can significantly reduce the fringe field effect in LCoS devices.

2. Device structure and theory

Figure 1 depicts the device configuration of protrusion located between the adjacent pixels in the high-resolution LCoS. In such a configuration, a polarizing beam splitter (PBS) is set in front of the top glass and its polarizer's axis is at 0°, indium-tim-oxide (ITO) as the common electrode is coated on the top glass substrate, and aluminum electrodes as the pixel electrodes are coated on the bottom silicone substrate. LC is sandwiched between the two substrates, and its twist angle is 90° (−20° to 70°). As evident from Fig. 1, d is the LC layer's thickness of the LCoS cell, l is the pixel size, and w_1 is the gap of pixels, w_2 and h are the width and the height of the protrusion, respectively.

*Project supported by the National Key Research and Development Program of China (Grant No. 2018YFB0703701) and the National Natural Science Foundation of China (Grant No. 61475042).

†Corresponding author. E-mail: sun_yubao@163.com

© 2021 Chinese Physical Society and IOP Publishing Ltd

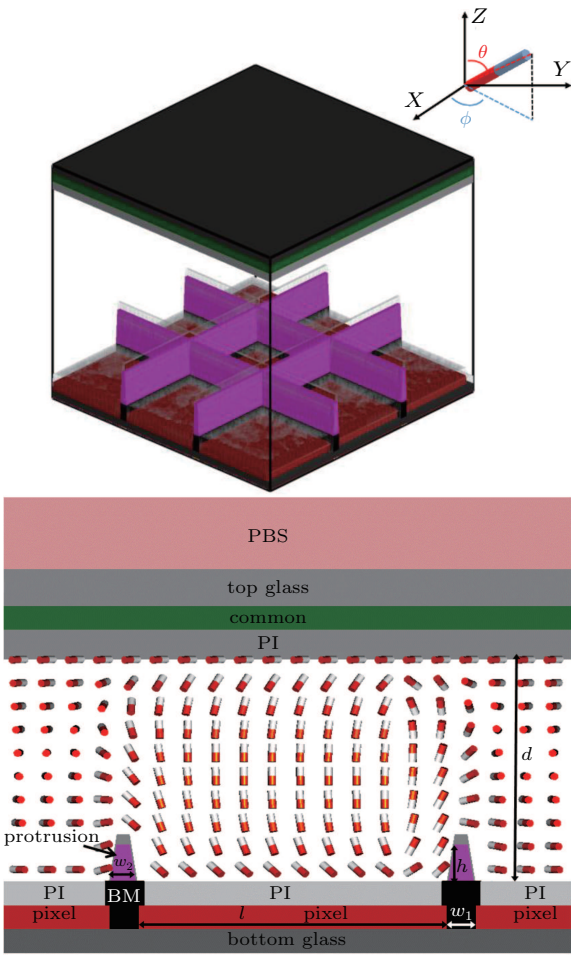


Fig. 1. Configuration of LCoS with protrusion located between the adjacent pixels.

In simulation, the extended Jones matrix method and Frank's continuum theory have been used to calculate the voltage-dependent reflectance.[32,36] For the off-state, the optical transmittance of the twisted LC layer can be described as[32]

$$M = \left|\cos\beta \ \sin\beta\right| \begin{vmatrix} \cos X - \mathrm{i}\frac{\Gamma}{2}\frac{\sin X}{X} & -\emptyset\frac{\sin X}{X} \\ \emptyset\frac{\sin X}{X} & \cos X + \mathrm{i}\frac{\Gamma}{2}\frac{\sin X}{X} \end{vmatrix} \times \begin{vmatrix} \cos X - \mathrm{i}\frac{\Gamma}{2}\frac{\sin X}{X} & \emptyset\frac{\sin X}{X} \\ -\emptyset\frac{\sin X}{X} & \cos X + \mathrm{i}\frac{\Gamma}{2}\frac{\sin X}{X} \end{vmatrix} \begin{vmatrix} -\sin\beta \\ \cos\beta \end{vmatrix}, \quad (1)$$

$$T = |M|^2, \quad (2)$$

where $\emptyset$ is the twist angle, β is the angle between the PBS polarization axis and LC alignment directions at the top surface. $X = \sqrt{\emptyset^2 + (\Gamma/2)^2}$ and $\Gamma = 2\pi\Delta n d/\lambda$, λ is the incident wavelength, and Δn is the birefringence of the liquid crystal. When $\beta = 20°$, 90° MTN cell has the maximum light efficiency[32] under the following condition:

$$2\Delta n d/\lambda = \sqrt{m^2 - 1/4}, \quad (m = 1, 2, 3, \ldots). \quad (3)$$

The maximum reflectance of the reflective-mode MTN is chosen at the first minimum,[37] $2\Delta n d/\lambda = \sqrt{3}/2$, for the thinnest LC thickness to obtain the fast response speed. A commercial simulation software TechWiz LCD 3D (Sanayi System Co., Ltd., Korea) is used to simulate the electro-optical properties.

In the simulation, the pretilt angle is 2°, the pixel's width is $l = 10$ μm, and its gap is varied from 0.5 μm to 0.8 μm. The LC material has $\Delta\varepsilon = 5.3$, $\Delta n = 0.096$ ($\lambda = 550$ nm), $d = 2.5$ μm, $K_{11} = 10.87$ pN, $K_{22} = 9.5$ pN, $K_{33} = 15.37$ pN. In order to obtain the high reflection and reduce the fringe field effect, the width of the protrusion (w_2) is varied from 0.5 μm to 0.9 μm, the height of the protrusion (h) is varied from 0.3 μm to 0.7 μm, and the dielectric constant is 4.0.

3. Results and discussion

From Fig. 2, there are two cases for the influence of the adjacent pixels: (a) the dark invalid pixel region (the region with $R < 0.1R_{\max}$ in bright pixel), and (b) the bright invalid pixel region ($R > 0.1R_{\max}$ in black pixel). In the sudoku pixels, the middle one is driven by the operate voltage to obtain the dark pixel (voltage-on pixel), and other eight pixels are named as the bright pixels (voltage-off pixels). The dark region extends into the adjacent bright pixel, we call the dark region in white pixel as the dark invalid pixel region, L_{1b} and L_{2b} are the X-direction widths of the dark invalid pixel region on the left and right sides of the voltage-on pixel. The total X-direction width of the dark invalid pixel region on both sides ($L_b = L_{1b} + L_{2b}$) is shown in Fig. 2(a). On the other hand, the bright region in the dark (voltage-on) pixel is called as the bright invalid pixel region, L_{1w} and L_{2w} are the X-direction widths of the bright invalid pixel region on the two sides. The total X-direction width of the bright invalid pixel region on both sides ($L_w = L_{1w} + L_{2w}$) is shown in Fig. 2(b). If $L_w > 0$, the dark state shows a serious light-leakage, this case can reduce the contrast ratio, so it needs to be eliminated at the first. When the height of the protrusion is small (less than 0.7 μm), there is only the inherent elasticity of the liquid crystal, the protrusion has a little effect on the LC alignment between adjacent pixels. When the height of the protrusion is

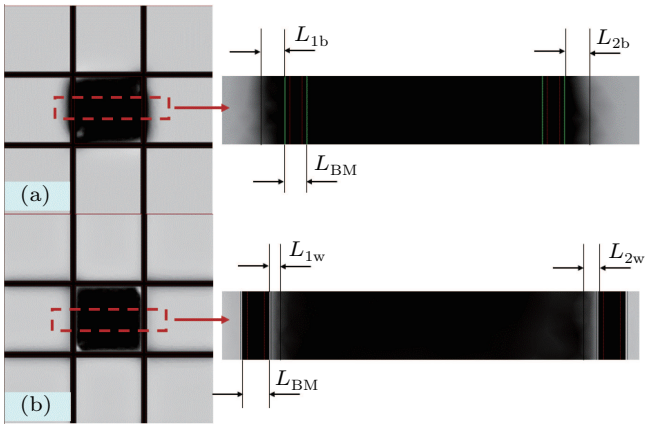


Fig. 2. The X-direction width of the invalid pixel region in normal-white mode. (a) The dark invalid pixel region for the protrusion with $h = 0.5$ μm and $w_2 = 0.5$ μm. (b) The bright invalid pixel region for the protrusion with $h = 2.0$ μm and $w_2 = 0.5$ μm.

larger than 0.7 μm in our simulation, most of the liquid crystal molecules are on two sides of the protrusion. The LC alignment and surface forces at the edges of the protrusion are the same as those on the substrates surface. The protrusion prevents the liquid crystal molecules from twisting in response to an electric field. When the pixel turns black with voltage applied, the region will appear white. From Fig. 2(b), the too large height of the protrusion leads to the bright invalid pixel region, so the height of the protrusion is chosen to be less than 0.7 μm for $L_w = 0$, the total invalid pixel region width L_t on the X-direction is written as

$$L_t = L_{1b} + L_{2b}. \tag{4}$$

To evaluate the electro-optic characteristics of 90°-MTN LCoS with a protrusion located between the adjacent pixels, we simulate the voltage-dependent reflectance of the cell, which has the protrusion with different heights from 0.3 μm to 0.7 μm and different widths from 0.5 μm to 0.9 μm. As shown in Fig. 3, the reflectance is influenced by the height and width of the protrusion, but its change is within 1.3%, and it is small enough to be regarded as the dark state when the voltage reaches 5 V. The off-state voltage (V_{off}) is 0 V and the on-state voltage (V_{on}) is 5 V. We simulate the X-direction reflectance (X–R) curves at $V_{on} = 5$ V to compare the invalid pixel regions of the cell with different heights and widths.

Figure 4 depicts the X–R curves for the protrusion with different heights from 0.3 μm to 0.7 μm and different widths from 0.5 μm to 0.9 μm. To avoid reducing the display area, the protrusion's width (the rectangle with solid line and gray black color) is not larger than the width of the black matrix (BM) (the rectangle with dashed line, 0.9 μm), where the protrusion width is varied from 0.5 μm (the pixel gap) to 0.9 μm (the

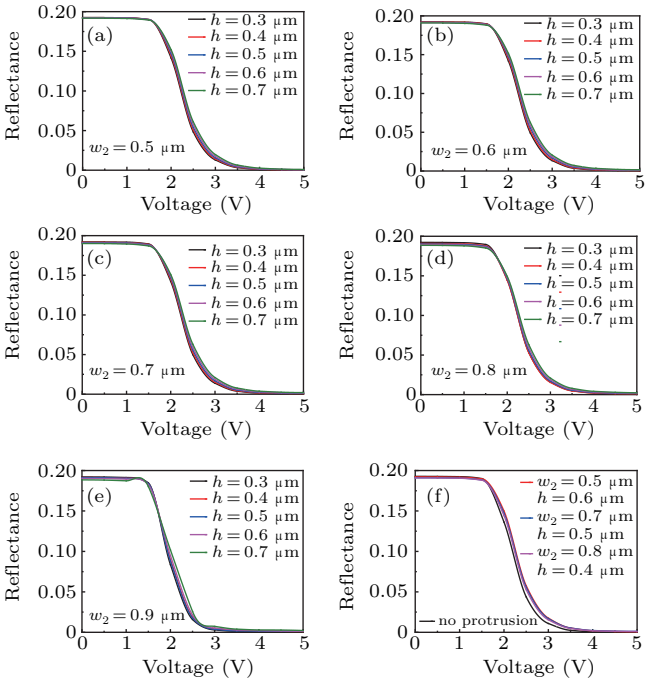


Fig. 3. Simulated V–R curves of the protrusion with different heights from 0.3 μm to 0.7 μm for (a) $w_2 = 0.5$ μm, (b) $w_2 = 0.6$ μm, (c) $w_2 = 0.7$ μm, (d) $w_2 = 0.8$ μm, (e) $w_2 = 0.9$ μm, and (f) compared with no-protrusion.

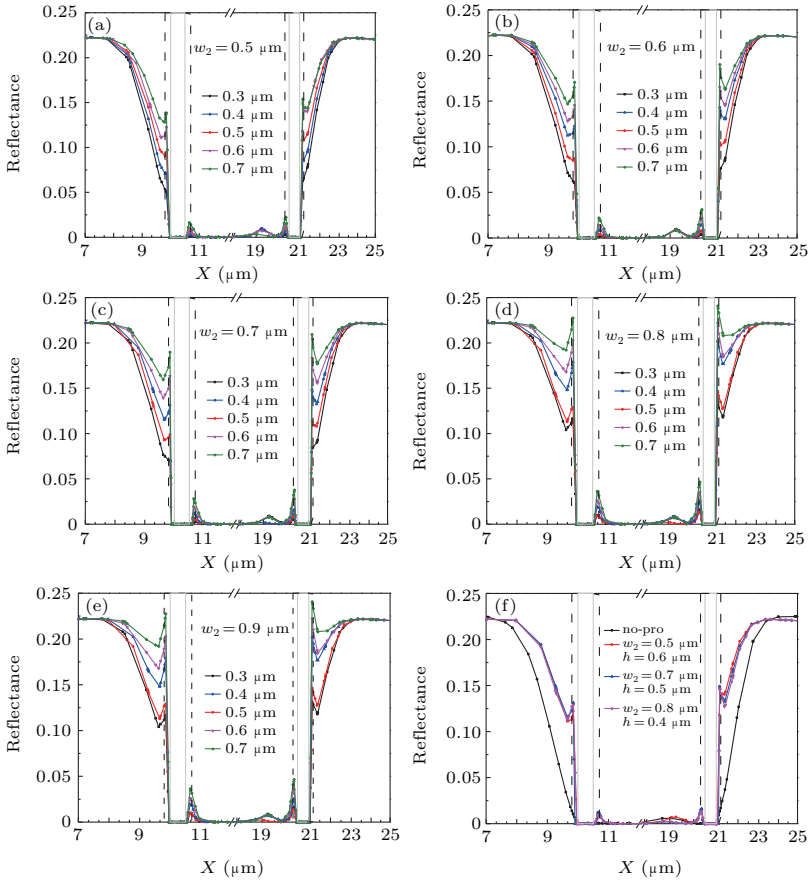


Fig. 4. Simulated X–R curves for different protrusion heights from 0.3 μm to 0.7 μm and (a) $w_2 = 0.5$ μm, (b) $w_2 = 0.6$ μm, (c) $w_2 = 0.7$ μm, (d) $w_2 = 0.8$ μm, (e) $w_2 = 0.9$ μm, (f) compare with no protrusion.

BM width). As no protrusion is used, the dark invalid pixel region in the adjacent bright (voltage-off) pixels is obvious, L_b is decreased as the protrusion's height increases from 0.3 μm to 0.7 μm for all above widths. Moreover, the reflectance at the edges of the protrusion in the dark pixel (voltage-off) increases with the increasing height of the protrusion because of the surface anchoring of the alignment layer on the protrusion and the inherent elasticity of the LC layer, as a result, L_w is not zero. For avoiding the bright invalid pixel region, the width of the protrusion is smaller than the BM's width, the height of the protrusion is also smaller than a critical value.

From Table 1, the total invalid pixel region width for the cell without protrusion is 3.345 μm, and it decreases as the protrusion height increases from 0.3 μm to 0.7 μm for the different protrusion widths (0.5 μm, 0.6 μm, 0.7 μm, 0.8 μm, 0.9 μm).

Table 1. The L_t for the SiO_2 protrusion with different heights and different widths.

w_2 (μm)	h (μm)	L_{1b} (μm)	L_{2b} (μm)	L_{1w} (μm)	L_{2w} (μm)	L_t (μm)
0	0	1.618	1.727	0.000	0.000	3.345
	0.3	1.480	1.432	0.000	0.000	2.912
	0.4	1.410	1.166	0.000	0.000	2.576
0.5	0.5	1.410	1.166	0.000	0.000	2.576
	0.6	1.212	1.081	0.000	0.000	2.292
	0.7	0.927	1.032	0.000	0.150	–
	0.3	1.480	1.166	0.000	0.000	2.645
	0.4	1.410	1.166	0.000	0.000	2.576
0.6	0.5	1.410	1.166	0.000	0.000	2.576
	0.6	0.779	1.166	0.000	0.168	–
	0.7	0.779	0.853	0.150	0.200	–
	0.3	1.480	1.166	0.000	0.000	2.645
	0.4	1.212	1.376	0.000	0.000	2.588
0.7	0.5	1.212	1.081	0.000	0.000	2.292
	0.6	0.779	1.166	0.150	0.200	–
	0.7	0.779	0.853	0.200	0.200	–
	0.3	1.410	1.166	0.000	0.000	2.576
	0.4	1.212	1.081	0.000	0.000	2.292
0.8	0.5	0.737	0.776	0.000	0.200	–
	0.6	0.779	0.853	0.200	0.200	–
	0.7	0.779	0.069	0.200	0.303	–
	0.3	1.410	1.166	0.000	0.000	2.576
0.9	0.4	1.212	1.081	0.000	0.200	–
	0.5	0.779	0.853	0.200	0.200	–

Based on $L_w = 0$, when $w_2 = 0.5$ μm, the height is less than 0.7 μm, L_t is decreased from 12.9% to 31.5% compared with that without protrusion as the protrusion height increases from 0.3 μm to 0.7 μm, and $L_w > 0$ when the protrusion height is larger than 0.7 μm. The L_t of the protrusion with $h = 0.6$ μm and $w_2 = 0.5$ μm is the smallest, 31.5% smaller than that without protrusion. When $w_2 = 0.6$ μm, the protrusion height needs to be less than 0.6 μm, and L_t is decreased from 20.9% to 23.0% as the protrusion height increases from 0.3 μm to 0.5 μm. When $w_2 = 0.7$ μm, the protrusion height needs to be less than 0.6 μm, and L_t is decreased from 20.9% to 31.5% as the protrusion height increases from 0.3 μm to 0.5 μm. When $w_2 = 0.8$ μm, the protrusion height needs to be less than 0.5 μm, and L_t is decreased from 23.0% to 31.5% as the protrusion height increases from 0.3 μm to 0.4 μm. When $w_2 = 0.9$ μm, the L_t with the protrusion of $h = 0.3$ μm is 23.0% smaller than that without protrusion. Hence, three sets of (h, w_2) with the smallest L_t are ($h = 0.4$ μm, $w_2 = 0.8$ μm), ($h = 0.5$ μm, $w_2 = 0.7$ μm), and ($h = 0.6$ μm, $w_2 = 0.5$ μm), the total width of the invalid pixel region is reduced by 31.5% compared with that of the cell without protrusion.[38]

The comparison of the liquid crystal distribution for the cells without and with protrusion ($h = 0.6$ μm $w_2 = 0.5$ μm) has been made, as illustrated in Fig. 5. When there is no wall protrusion between the adjacent pixels, the pixel shows the rounded edges at the left and right sides, so the dark invalid region is large. When the protrusion with 0.5 μm width and 0.6 μm height is located between the adjacent pixels, the dark invalid region is reduced more, and few smaller bright invalid regions exist at the corners of the black pixels ($L_w \approx 0$).

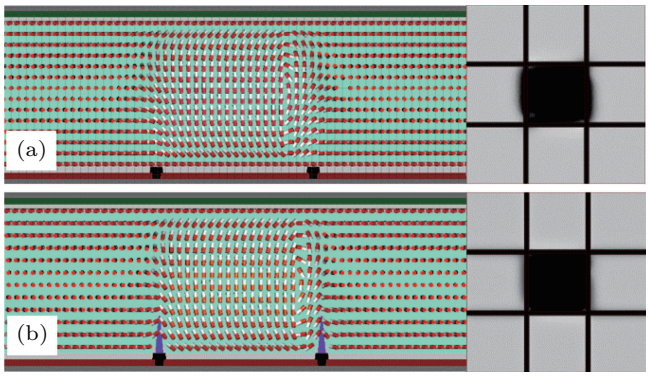


Fig. 5. The arrangement of liquid crystal and simulated image for the cell (a) without protrusion, and (b) with protrusion ($h = 0.6$ μm $w_2 = 0.5$ μm).

4. Conclusion

The total invalid pixel region width of an MTN-LCoS with different protrusion's widths and heights is calculated. The results indicate that the total invalid pixel region width can be reduced by 31.5% with the suitable protrusion's width and height, so the contrast ratio can be improved. The protrusion can be fabricated by the traditional photoresist development method or nanoimprinting method,[35] which matches the photolithography process. The material can be chosen as the organic material, such as photoresist, which has good softness and is not fragile. These results have an important influence on improving the electro-optic characteristics of LCoS.

References

[1] Boccardi F, Heath J R W, Lozano A, Marzetta T L and Popovski P 2014 *IEEE Comm. Mag.* **52** 74
[2] Lee H S, Jang S, Noh J, Jeon H and Kim S 2017 *SID Symp. Dig. Tech. Pap.* **48** 403
[3] Li R, Chu F, Dou H, Tian L L and Wang Q H 2019 *SID Symp. Dig. Tech. Pap.* **50** 1800
[4] Won Y, Seo E J and Lim Y J 2019 *SID Symp. Dig. Tech. Pap.* **50** 1802

[5] Vieri C, Lee G, Balram N, Jung, S H, Yang J Y, Yoon S Y and Kang I B 2018 *J. Soc. Inf. Disp.* **26** 314

[6] Katayama T, Higashida S, Kanashima A, Hanaoka K and Yoshida H 2019 *SID Symp. Dig. Tech. Pap.* **49** 671

[7] Shi L, Srivastava A K and Cheung A 2018 *J. Soc. Inf. Disp.* **26** 325

[8] Lu L, Peng F L, Wang M F, McEldowney S and Silverstein B 2019 *SID Symp. Dig. Tech. Pap.* **50** 826

[9] Chen C H 2015 *Handbook of digital imaging* (New York: John Wiley & Sons Ltd) pp. 1–20

[10] Li P K 2018 *Information Display* **34** 12

[11] Tsai C W 2018 *SID Symp. Dig. Tech. Pap.* **49** 218

[12] Zhu X and Wu S T 2004 *J. Appl. Phys.* **95** 7660

[13] Cuypers D, De Smet H, De Smet J, Joshi P, Shang X and Van Calster A 2014 *J. Soc. Inf. Disp.* **22** 457

[14] Hyman R M, Lorenz A and Wilkinson T D 2015 *Liq. Cryst.* **43** 83

[15] Luo Z, Peng F, Chen H, Hu M and Wu S T 2015 *Opt. Mater. Express* **5** 603

[16] Chen H W, Gou F W and Wu S T 2017 *SID Symp. Dig. Tech. Pap.* **48** 377

[17] Chen R, Huang Y, Li J, Hu M and An Z 2018 *Liq. Cryst.* **46** 309

[18] Xing Y F, Guo Z B and Li Q 2018 *Liq. Cryst.* **45** 507

[19] Fan K H, Wu S T and Chen S H 2006 *J. Disp. Technol.* **1** 304

[20] Apter B, Efron U and Bahat-Treidel E 2004 *Appl. Opt.* **43** 11

[21] Fan Chiang K H, Zhu X, Wu S Tand Chen S 2005 *SID Symp. Dig. Tech. Pap.* **36** 1290

[22] Zhang Y, Wang B, Chung D B, Colegrove J and Bos P J 2012 *SID Symp. Dig. Tech. Pap.* **36** 1178

[23] Li Y W, Fan-Chiang K H, Wang C T, Chia T and Hung-Chien Y 2012 *SID Symp. Dig. Tech. Pap.* **43** 914

[24] Nie Z, Day S E, Fernandez F A, Willman E and James R 2014 *SID Symp. Dig. Tech. Pap.* **45** 1382

[25] Lu T X, Pivnenko M, Robertson B and Chu D P 2015 *Appl. Opt.* **54** 5903

[26] Isomae Y, Shibata Y, Ishinabe T and Fujikake H 2016 *SID Symp. Dig. Tech. Pap.* **47** 1670

[27] Isomae Y, Ishinabe T, Shibata Y and Fujikake H 2019 *SID Symp. Dig. Tech. Pap.* **50** 66

[28] Cuypers D, Smet H D and Calster A V 2007 *J. Soc. Inf. Disp.* **15** 775

[29] Vanbrabant P J M, Beeckman J, Neyts K, Willman E and Fernandez F A 2010 *J. Appl. Phys.* **108** 083104

[30] Peng F L, Gou F W, Chen H W, Huang Y G and Wu S T 2016 *J. Soc. Inf. Disp.* **24** 241

[31] Fan K H F, Wu S T and Chen S H 2002 *Jpn. J. Appl. Phys.* **41** 4577

[32] Wu S T and Wu C S 1996 *Appl. Phys. Lett.* **68** 1455

[33] Yang J P, Chen H M P, Huang Y, Chang Y C and Hsu R 2019 *SID Symp. Dig. Tech. Pap.* **50** 993

[34] Baek J I, Shin J H, Oh M C, Kim J C and Yoon T H 2006 *Appl. Phys. Lett.* **88** 161104

[35] Isomae Y, Ishinabe T, Shibata Y and Fujikake H 2019 *J. Soc. Inf. Disp.* **27** 251

[36] Wu S T 2001 *Reflective Liquid Crystal Displays* (New York: John Wiley & Sons Inc) p. 427

[37] Gooch C H and Tarry H A 1975 *J. Phys. D: Appl. Phys.* **8** 1575

[38] Chen Y, Peng F L, Wu S T, Mo L C and An Z W 2014 *SID Symp. Dig. Tech. Pap.* **44** 898